Supplemental Document

Biomedical Optics EXPRESS

Cellular analysis using label-free parallel array microscopy with Fourier ptychography: supplement

DEVIN L. WAKEFIELD,[1,3,*] RICHARD GRAHAM,[2,3] KEVIN WONG,[2,3] SONGLI WANG,[1] CHRISTOPHER HALE,[1] AND CHUNG-CHIEH YU[2]

[1]*Amgen Inc, South San Francisco, CA 94080, USA*
[2]*Clearbridge Biophotonics FPM Inc, Pasadena, CA 91101, USA (no longer in operation)*
[3]*These authors contributed equally to this work*
[*]*dwakefie@amgen.com*

This supplement published with Optica Publishing Group on 7 February 2022 by The Authors under the terms of the Creative Commons Attribution 4.0 License in the format provided by the authors and unedited. Further distribution of this work must maintain attribution to the author(s) and the published article's title, journal citation, and DOI.

Supplement DOI: https://doi.org/10.6084/m9.figshare.19102208

Parent Article DOI: https://doi.org/10.1364/BOE.451128

Cellular Analysis using Label-Free Parallel Array Microscopy with Fourier Ptychography: supplemental document

1. FPM DATASET

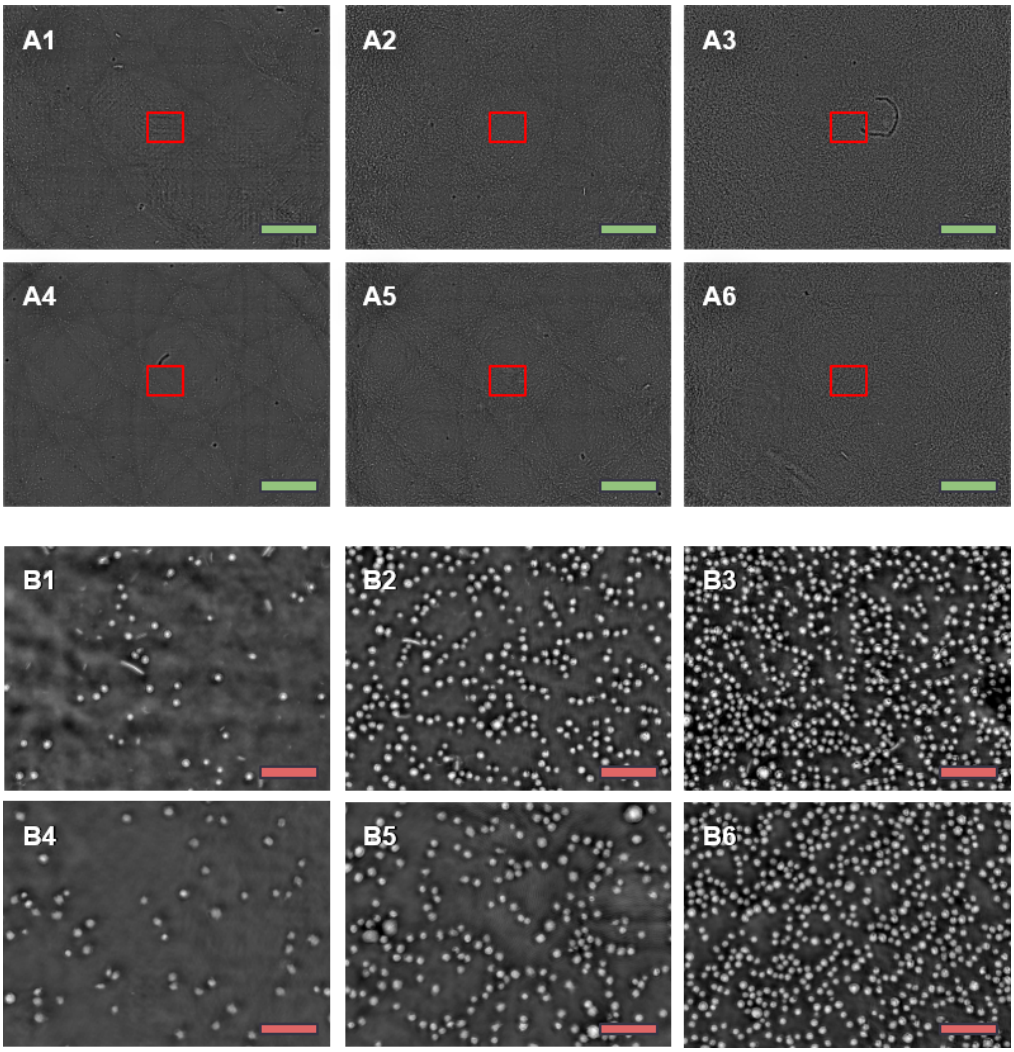

Fig. S1. Example 6-well microplate with different T-cell densities imaged on the *SimulPhi-6* system. All images in this figure were captured after fixation. Images A1 to A6 show full field of views for wells 1 to 6, respectively. Low, medium, and high cell densities are captured in the left column (A1 and A4), the middle column (A2 and A5), and the right column (A3 and A6), respectively. Images B1 to B6 show zoomed-in regions from images A1 to A6, respectively, as indicated by the red rectangles. Green scale bars represent 1 mm. Red scale bars represent 100 μm.

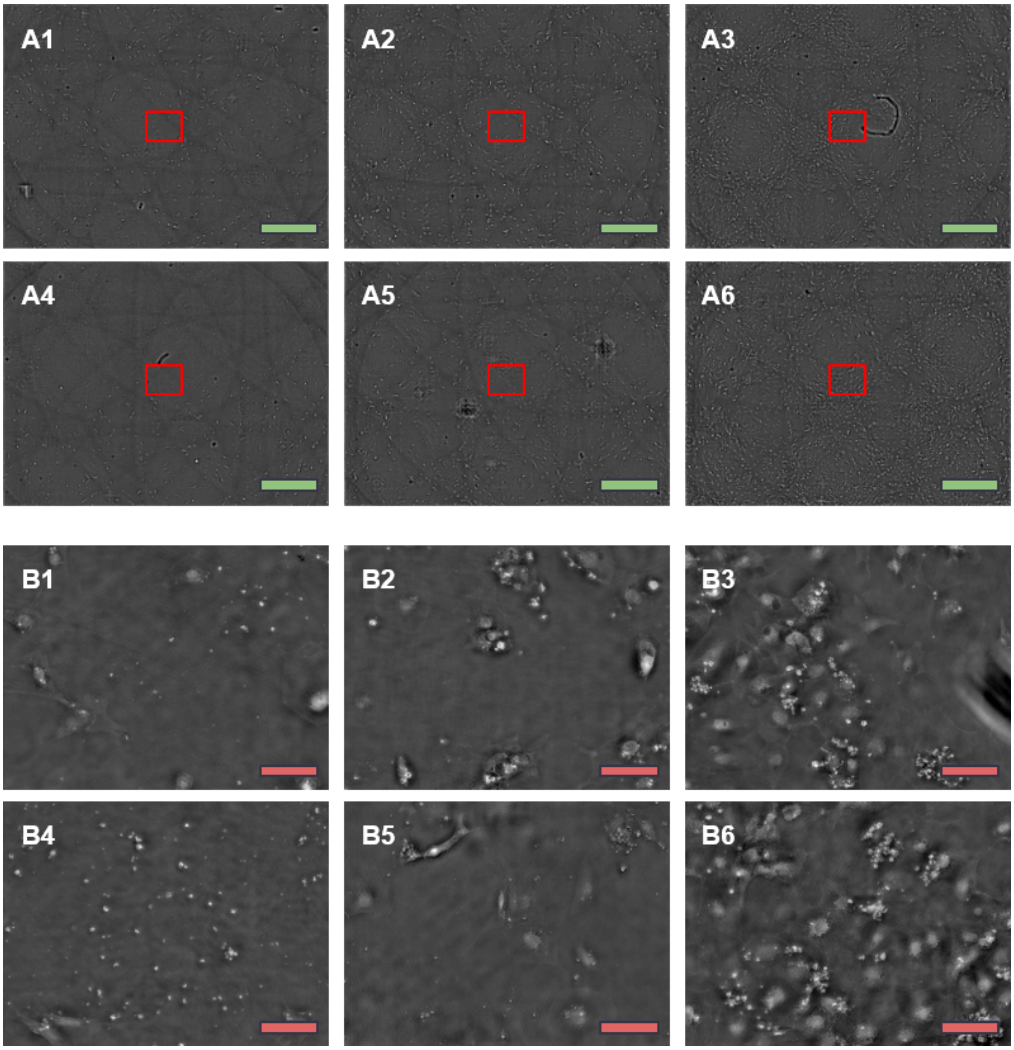

Fig. S2. Example 6-well microplate with different iPSC-CM densities imaged on the *SimulPhi-6* system. All images in this figure were captured after fixation. Images A1 to A6 show full field of views for wells 1 to 6, respectively. Low, medium, and high cell densities are captured in the left column (A1 and A4), the middle column (A2 and A5), and the right column (A3 and A6), respectively. Images B1 to B6 show zoomed-in regions from images A1 to A6, respectively, as indicated by the red rectangles. Green scale bars represent 1 mm. Red scale bars represent 100 μm.

2. FPM ARTIFACTS

It is noteworthy that while the features described in the Section 5.2 can be used to improve the segmentation and cell counting from FPM data, some exist to mitigate the effects of FPM artifacts. These artifacts should not exist in an ideal quantitative phase modality, but are seen in the present system. The most common artifacts are illustrated in Figure S3 and include:

1. Variations in the background level in different FPM reconstructions.
2. High spatial-frequency 'wavy' artifacts. Present in some tiles, especially near the edge of the field of view.
3. Phase-wrap artifacts from thick samples.
4. Characteristic large cross-pattern artifacts due to floating debris outside the working focal range.
5. Large scale 'overlapping rings' illumination artifacts.
6. High spatial frequency 'fuzz' artifacts. These are suspected to be due to motion within the sample during acquisition and/or very thick regions of a sample.

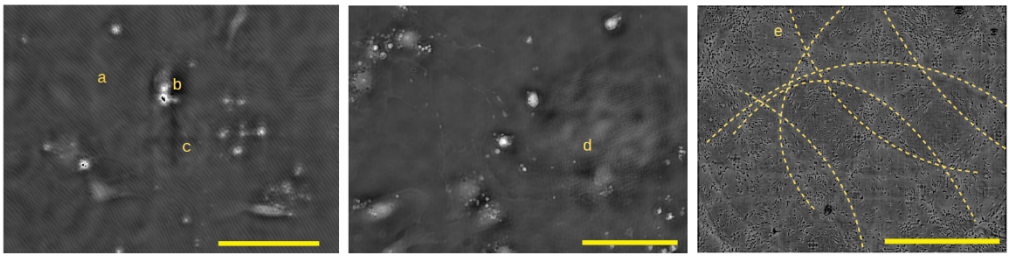

Fig. S3. Illustration of selected FPM artifacts. Left and center images are from an iPSC-CM sample. Right image is a large FOV from a U2OS sample. Artifacts shown include (a) wavy artifact, (b) phase-wrap, (c) cross-pattern, (d) high spatial frequency fuzz, and (e) overlapping rings illumination artifact. The right image has been processed to artificially modify the intensity to more clearly show the illumination artifact, some examples of which have also been outlined with yellow dashed lines. From left to right, scale bars represent 100 μm, 100 μm, and 400 μm.

3. DPC AND FPM COMPARISONS

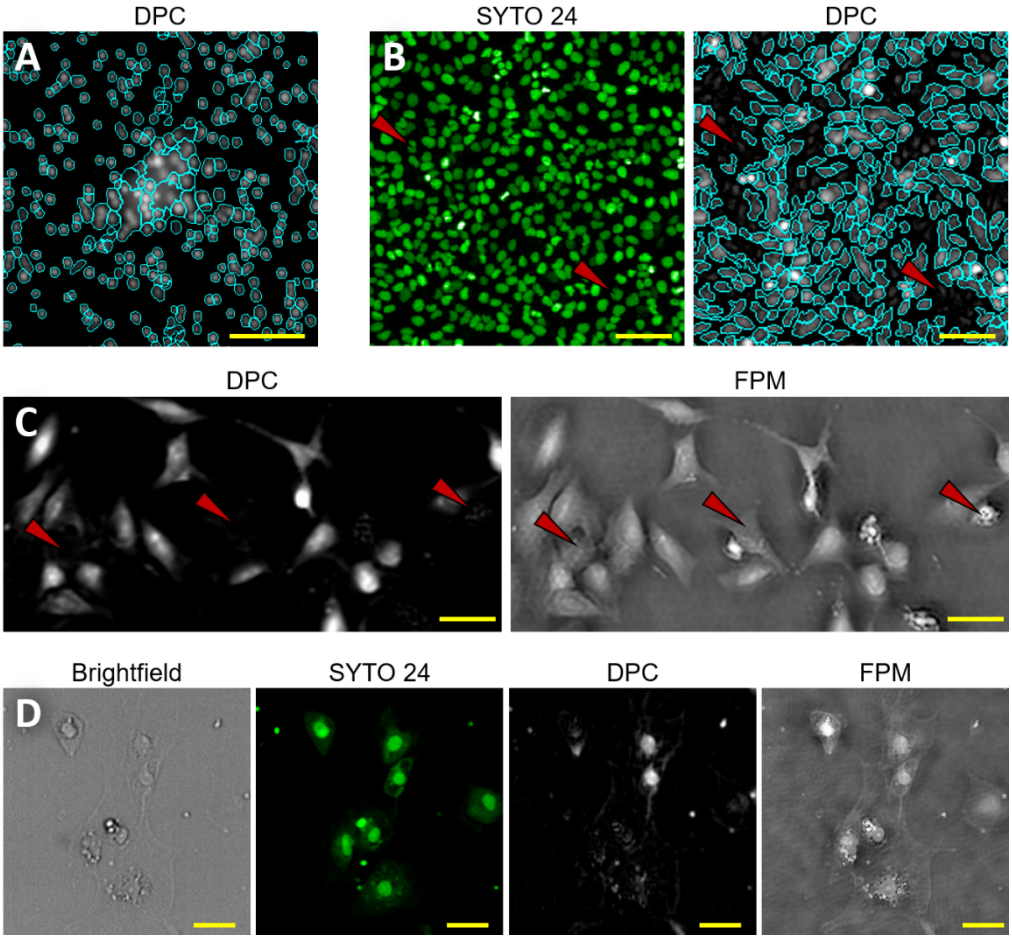

Fig. S4. Selected examples comparing differences in imaging modalities and where FPM captures cells with better definition and contrast than DPC. (A) Jurkat T-cells, in the middle of this DPC image, are in contact with large debris and are not well segmented in Columbus™. (B) U2OS cells seeded at high density are readily detectable via fluorescent imaging (left) but when imaged via DPC, a number of these same cells present a challenge for Columbus™ DPC segmentation, largely due to low contrast (right). A few specific examples are denoted by red arrows. (C) Illustrated by the red arrows, multiple U2OS cells are missing or are poorly detected by DPC (left) whereas these same cells are clearly visible in the FPM image (right). (D) Similarly, FPM readily captures the diversity of cell morphologies and thicknesses, offering clear help toward individual iPSC-CM cell segmentation and counting. Several thin iPSC-CM cells do not show up in DPC image here but are noticeably visible in other imaging modalities, and with the most detail in the FPM image. All scale bars represent 50 μm, with the exception of B with 25 μm scale bars.

4. AUTOMATED VOLUME THRESHOLD DETERMINATION

Figure S5 illustrates the automated method used here to determine an appropriate volume threshold in an unbiased and automated way given a large set of example data for a particular cell type. Note that the method used here differs from the gamma function curve fitting technique presented by Loewke *et. al* 2018 [1].

Consider first the case in which segmentation is run with v_{th} set to represent a significantly larger volume than is realistic for representing the minimum viable nucleus volume of a particular cell type (Figure S5A green line). Segmentation contours will be drawn extending unrealistically beyond the actual boundaries of the nucleus. Over the whole population we should expect a slight reduction in cell counts because nearby neighboring cells have been inappropriately merged. The overall decrease in cell counts is however relatively slight, especially for samples at moderate seeding density. This effect is not biased to any particular cell size and will tend to skew the final distribution of identified cells towards a larger average volume.

Consider next the case in which segmentation is run with v_{th} significantly smaller than realistic (Figure S5A blue line). In this case, the segmentation will incorrectly break otherwise valid, uniform nuclei regions into smaller parts along arbitrary dividing boundaries. The outer regions of the nucleus will generally be identified to fall within the cytoplasm, which is segmented using a secondary flood-filling technique. While the total number of cells will again generally remain comparable to those with segmentations based on a more realistic v_{th}, a histogram will reveal that the population shows an excess of small cells, where the segmented nuclear volume is limited by the v_{th} setting, rather than the natural underlying volume distribution.

'Small cells' are classified as those with volumes near the cut-off v_{th}. The threshold for 'near' can be set manually and the technique is not especially sensitive to the exact value. The cells counted with and without this classification are shown in Figure S5B for segmentations with varying v_{th}. Figure S5C shows the same data in fractional form.

Overall, two effects are present here, each of which reduce the number of cells falling in the extreme left of the cell volume histogram (simply classed as 'small' cells here) when the v_{th} setting is increased. Yet, these are independent effects. The first occurs simply through the segmentation becoming more representative of the underlying distribution, and is quite aggressive. The second is less aggressive and skews the distribution, inappropriately reducing the 'small' fraction. It is therefore possible to identify a 'knee' in Figure S5C due to the complementary but distinct effects. This can be done automatically with a simple bilinear least-squares fit. The intersection point then can be adopted at the appropriate v_{th} value since the value for which the cell volume distribution is not limited by the selected v_{th}. An example showing segmentations of a typical region of moderate density U2OS sample at the discussed low, near ideal, and high v_{th} setting is shown in Figure S6.

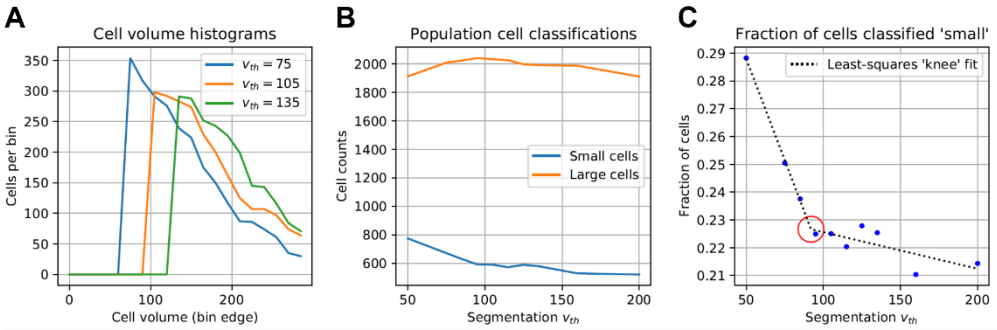

Fig. S5. Plots demonstrating the procedure used to automatically determine a volume threshold for a cell population. Data is from an acquisition of live U2OS cells at moderate seeding density. (A) Cell volume histograms for three example v_{th} values. (B) Cell counts categorized over a range of v_{th} values, in which 'small' represents the cells in the left most region of the histogram (volumes within 30 ± 10 units of v_{th}). (C) The fraction of all cells falling within the 'small' classification for multiple runs, with a least-squares 'knee' fit. At the 'knee' point (red circle, here 92 ± 7 units) the threshold is most representative of the underlying cell population.

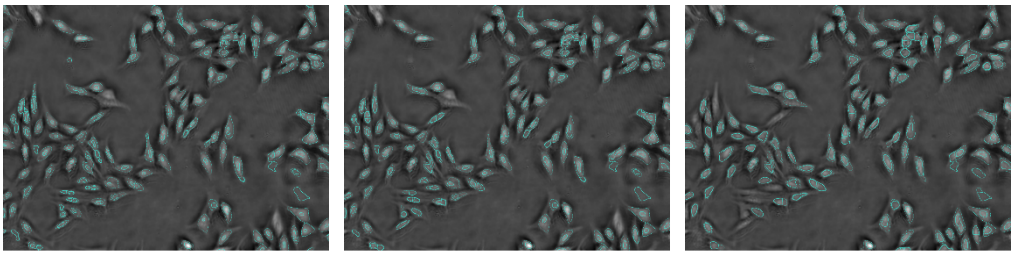

Fig. S6. Example segmentations of U2OS cells under excessively low, high, and near ideal v_{th} settings. Note that the automated exclusions discussed elsewhere have not been applied to these examples so as to show only the effect of varying the v_{th}. A production segmentation made with these enabled would typically remove outliers such as the occasional very sparse 'empty' cells and cells with no cytoplasm differentiated from any nucleus region.

REFERENCES

1. N. O. Loewke, S. Pai, C. Cordeiro, D. Black, B. L. King, C. H. Contag, B. Chen, T. M. Baer, and O. Solgaard, "Automated cell segmentation for quantitative phase microscopy," IEEE transactions on medical imaging **37**, 929–940 (2018).